# Protostellar Jets and Turbulence in Molecular Clouds: The Role of Interactions

Andrew J. Cunningham[1], Adam Frank[2], Eric G. Blackman[3]

*Department of Physics and Astronomy, University of Rochester, Rochester, NY 14620*

## ABSTRACT

We present a series of numerical studies of the interaction of colliding radiative, hydrodynamic young stellar outflows. We study the effect of the collision impact parameter on the acceleration of ambient material and the degree to which the flow is isotropized by the collision as a mechanism for driving turbulence in the parent molecular cloud. Our results indicate that the high degrees of compression of outflow material, achieved through radiative shocks near the vertex of the interaction, prevents the redirected outflow from spraying over a large spatial region. Furthermore, the collision reduces the redirected outflow's ability to entrain and impart momentum into the ambient cloud. Consideration of the probabilities of outflow collisions leads us to conclude that individual low velocity fossil outflows are the principle coupling between outflows and the cloud.

*Subject headings:* ISM: jets and outflows; ISM: clouds; turbulence

## 1. Introduction

Molecular Clouds have long been a subject of interest in astrophysics since they are the exclusive environments in which stars form in galaxies. The expected lifetimes for molecular clouds has become a topic of considerable debate as numerical simulations have shown that MHD turbulence, the nominal means of support for the clouds against self-gravity, will decay on a crossing timescale (Mac Low et al. 1998; Stone et al. 1998; Vazquez-Semadeni et al. 2000). In light of this result it is difficult to understand why molecular clouds do not fully collapse in an efficient burst of star formation on timescales no longer than a few

[1]ajc4@pas.rochester.edu

[2]afrank@pas.rochester.edu

[3]blackman@pas.rochester.edu

crossing times. Thus it appears that either molecular clouds are transient features or they are resupplied with turbulent energy through some other means.

Jets and molecular outflows are recognized as a ubiquitous phenomena associated with star formation. It is expected that most if not all low mass stars produce a collimated outflow during their formation from a parent molecular cloud core (massive stars may also produce collimated outflows though this point remains somewhat speculative (Shepherd 2003)). Stars do not, however, form in isolation. Rich star forming regions such as Orion can contain as many as 1000 stars per $pc^3$ (Testi et al. 1999). Low mass star forming regions such as Taurus or Perseus will contain hundreds of stars in a similar volume.

The ubiquity and high density of outflows from young stars make them an intriguing candidate for the source of turbulent energy in molecular clouds. The idea that feedback from TT winds could lead to a self-regulating state of star formation dates back as far as Norman & Silk (1980). Consideration of combined energy budget for the outflows in some clouds compared with the energy in the cloud's turbulent motions support notions of feedback showing an approximate balance between outflow input and turbulent support Bally et al. (1996); Bally & Reipurth (2001); Knee & Sandell (2000); Matzner (2002); Warin et al. (1996). Thus the combined action of many outflows could, in principle, provide the required deposition of turbulent energy to support a cloud against collapse. More recent observational studies have explored multiple (though apparently) non-interacting outflow structures in individual clouds and come to similar conclusions. For example direct observational evidence showing that the giant stellar outflows associated with HH 300 and HH 315 have disrupted their cloud's density and velocity distributions at parsec scale distances from their source has been provided by Arce (2003). The actual global disruptive effect these individual flows have depends on the ability that these outflows have to impart their momentum into their parent clouds by entraining and accelerating molecular gas (Arce 2003; Arce & Goodman 2001).

While invoking jets and outflows to drive turbulent motions appears attractive for molecular cloud studies, there is a potential problem with such a scenario. The principle means of energy transfer from jet to cloud appears to come via shock waves, the so-called "prompt entrainment" mechanism Chernin et al. (1994). This is to be compared with "turbulent entrainment" mechanism which occurs via a turbulent boundary at the edge of a jet Canto & Raga (1991). Thus the effect of a single supersonic outflow is bounded by the shock wave which defines it. Only those regions of a cloud which have been swept over by the outflow will gain any energy. Given such a localization of energy and momenta deposition, the action of multiple, isotropically oriented outflows is required to drive the random motions associated with isotropic turbulence. Somehow the energy and momenta in the localized

region engulfed by a jet or outflow must be randomized and distributed over many scales. The results presented here consider the facility of the collision of two protostellar outflows toward this result. We consider the interaction of two heavy jet flows oriented at 90 ° to each other with different impact parameters. Our goals in this study are to examine the resultant flows and attempt to distinguish between those with low and high impact parameters in terms of how ambient gas is accelerated.

## 2. Motivation

We estimate the probability that two protostellar outflows interact as a function of protostellar density in the cloud. We consider a volume $V$ that contains an average outflow density $N$ and assume that each protostar emits a bipolar outflow. We approximate the volume of these bipolar outflows as that of a cylindrical column of length $L$ and radius $R$. The outflow fill ratio $\frac{V_{outflow}}{V} = \pi R^2 L N$ provides an estimate of the volume fraction of the cloud that is occupied by outflows. Assuming that the production frequency of outflows in the cloud is constant we can cast the density of outflows active at any given instant in terms of the stellar density $N_*$ as $N = N_* \frac{t_{outflow}}{t_{cloud}}$. The probability two active outflows occupy the same region of space in the cloud at the same time is then $P \sim \left[\frac{V_{outflow}}{V}\right]^2$. Solving for $N_*$, we have

$$N_*(P) = \frac{\sqrt{P}}{\pi R^2 L} \frac{t_{cloud}}{t_{outflow}}. \tag{1}$$

We define $N_{critical}$ as the protostellar density that achieves a volume fill ratio of 10% bow-shock overlap $N_{critical} \equiv N(0.1)$. Above this intersection probability we expect the effect of collisions to become appreciable. We assume values for the typical protostellar outflow size as $L = 1$ pc, bow shock radius $R = R_{bs} = 0.1$ pc, outflow lifetime $t_{outflow} = 2 \times 10^5$ yr, and cloud lifetime $t_{cloud} = 10^7$ yr (Palla & Galli 1997). These values yield a stellar density $N_{critical} = 500$ pc$^{-3}$. This is comparable to the protostellar density of many star forming regions. Outflow interactions are therefore statistically likely to occur in a typical star forming region.

If the collision of outflow streams from adjacent YSO's contribute to the turbulent energy budget of their parent cloud, it would do so by increasing the rate at which the flow imparts momentum into the surrounding molecular gas. This could occur if the redirected outflow has a volume greater than the individual outflows. Also if the redirected flow generates more "splatter", in the sense that a wider range of scales become energized though vortices generated during the collision, then the increased rate of momentum deposition into the

ambient molecular gas would result in an increased rate of generation of turbulent energy and could thereby provide support for the parent cloud against gravitational collapse and star formation.

Beyond the issue of driving turbulence, the interaction of jets and outflows is of interest in its own right. While the propagation of single jets and outflows has received considerable attention (Lee et al. 2001; Ostriker et al. 2001) and seems to be fairly well understood, as is their interaction with clumps (Raga & Canto 1995) and side winds (Lebedev et al. 2004), the interaction *between* such flows is relatively unexplored.

## 3. Computational Method and Initial Conditions

### 3.1. Method: Numerical Code

In order to explore the efficacy of jet and outflow collisions at stirring the ambient media we have carried out a series of simulations using simplified initial conditions. In our study we have carried forward hydrodynamic simulations of the interaction of two orthogonal outflows. Our simulations include the effect of radiative energy loss on the flow. We investigate the role of impact parameter and degrees of collimation. Our simulations are carried out in 3D using the AstroBEAR adaptive mesh refinement (AMR) code. AMR allows high resolution to be achieved only in those regions which require it due to the presence of steep gradients in critical quantities such as gas density. The hydrodynamic version of AstroBEAR has been well tested on variety of problems in 1, 2, 2.5D (Poludnenko et al. 2005; Varnie et al. 2005) and 3D (Lebedev et al. 2004).

The BEARCLAW framework on which AstroBEAR is based has been recently extended to allow efficient parallel computation using MPI on distributed memory systems by combining two load balancing techniques:

- Domain Decomposition: The root level is divided into an arbitrary number of subdomains which are balanced across the processors.
- Dynamic Load Balancing: Each refined grid block is created on the same processor as its parent grid. Grids are moved to a lesser loaded processor at the beginning of each time step if such a move will reduce the average computational load (measured in CPU time) across the processors. This algorithm minimizes inter-processor communication and overhead and allows efficient load balancing even in cases where the implicit source term integration requires many iterations to converge in localized regions of the domain.

Domain decomposition alone cannot achieve efficient load balancing in the common situation where refined regions are confined to a small region of the domain. Dynamic balancing of the grid blocks can fail in cases where the number of refined grids on any level is less than the number of available processors. The combined parallelization strategy we have employed using both AMR load balancing and domain decomposition avoids these problems.

For the results presented here, AstroBEAR integrates the system of equations, $d_t Q + d_x F_x + d_y F_y + d_z F_z = S$. The vector of conserved quantities $Q$, the flux function $F$, and the micro-physical source terms $S$ are given as:

$$Q = \begin{bmatrix} \rho \\ \rho v_x \\ \rho v_y \\ \rho v_z \\ E \\ \rho_w \end{bmatrix}, F_* = v_* \begin{bmatrix} \rho \\ \rho v_x \\ \rho v_y \\ \rho v_z \\ E + P \\ \rho_w \end{bmatrix}, S = \begin{bmatrix} 0 \\ 0 \\ 0 \\ 0 \\ -\left(\frac{\rho}{\mu_H}\right)^2 \lambda \\ 0 \end{bmatrix},$$

where $\rho$ is the gas density, $v_x$, $v_y$ and $v_z$ are the Cartesian components of the velocity, $E$ is the total energy, $P$, is the gas pressure, $\rho_w$ traces the density of injected outflow material and $\mu_H$ is the atomic weight of hydrogen. The equation of state used is that of a monotonic ideal gas. While AstroBEAR is equipped with the capability to track the ionization and chemistry associated with a number of elements (Cunningham et al. 2005), we have, for computational efficacy, elected not to utilize these in the present calculations due to their high cost. What matters for our calculations is only the presence of time-dependent cooling behind shocks. As we will see the presence of cooling has a profound effect on the resulting flow patterns. We do not, however, require a detailed treatment of the ionization dynamics or chemistry to see these effects and so we have constructed a cooling function that mimics the effects of low temperature molecular cooling. This is an alternative to tracking full non-equilibrium molecular dissociation and cooling. Our cooling function (figure 1) is given by:

$$\lambda(T) = \lambda_{LS}(\chi, T) + \lambda_{DM}(T)$$

$$\chi(T) = \begin{cases} 0 & \text{for } T \leq 3000 \text{ K} \\ \min\left(\frac{T - 3000\ K}{7000\ \text{K}},\ 0.9\right) & \text{for } 3000 \text{ K} < T < 12600 \text{ K} \\ 1 & \text{otherwise} \end{cases}$$

where $\lambda_{DM}$ is the atomic line cooling function of Dalgarno & McCray (1972), $\lambda_{LS}$ is the molecular cooling function of Lepp & Schull (1983) for a hydrogen gas of density $10^4$ cm$^{-3}$ with a fraction of H atoms in the molecular state $1 - \chi$.

The calculations discussed here have been carried out using a spatial and temporal second order accurate MUSCL scheme using a Roe-average linearized Riemann solver. The

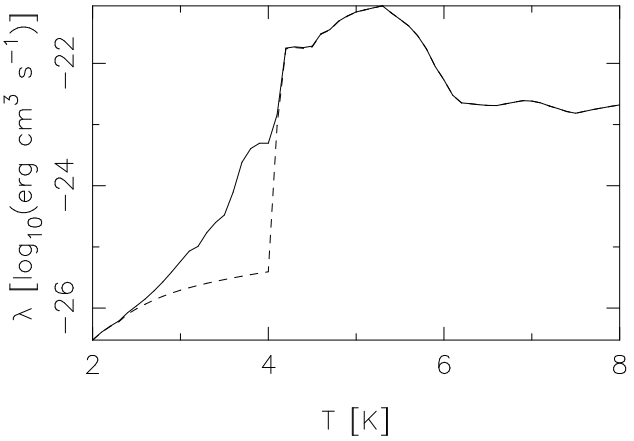


Fig. 1.— The full cooling curve including low temperature contributions $\lambda$ (solid line) and the atomic line cooling function of Dalgarno & McCray (1972)(dashed line).

MUSCL scheme employed here achieves second order spatial accuracy by performing a MINMOD interpolation of the primitive fields (density, velocity and pressure) to grid interfaces. The TVD-preserving time stepping method of Shu & Osher (1988) is used to advance the solution. The micro-physical source terms are handled separately from the hydrodynamic integration using an operator split approach. The source term is integrated using an implicit fourth-order Rosenbrock integration scheme for stiff ODE's. We have made use of the Local Oscillation Filter method of Sutherland et al. (2003) using a viscosity parameter $\alpha = 0.025$ to eliminate numerical instabilities that can occur near strongly radiative shock fronts.

### 3.2. Model: Colliding Jet Simulations

We have carried out a series of six simulations to investigate the capacity for two interacting outflows to excite motions on a range of scales and the efficacy with which they accelerate ambient gas. The parameters that are common to all of the simulations are given in table 1. Our computations are carried forward with a base grid that resolves the jet inflow with two cells per jet radius. Three levels of AMR refinement, each with a refinement ratio of two, produce and effective resolution of 16 computational cells per jet radius. The flows in these simulations are characterized by strong cooling, typical for YSO outflows. We characterize the strength of the cooling by defining a cooling parameter $\sigma$ which is the ratio of $\tau_{cool}$, the time for post shock ambient material to cool to $10^4$ K, to $\tau_{cross}$,the time for post shock ambient material to cross $r_j$. Typical values for YSO jets and outflows are such that flows with $\sigma << 1$ are expected. For the parameters chosen here, the cooling parameter is given by $\sigma = \tau_{cool}/\tau_{cross} \approx 0.01$.

Each simulation consists of two identical orthogonal jets. The jets are launched into domain via fixed cells embedded within the boundary. In the fixed cells the outflows maintain a uniform density and temperature. We use a velocity distribution characterized by a shear parameter $s$ and spray angle $\psi$:

$$\alpha(r) = 1 - (1 - s)\left(\frac{r}{r_j}\right)^2$$
$$v_{\parallel}(r) = v_j \alpha(r) \cos(\frac{r}{r_j}\psi)$$
$$v_{\perp}(r) = v_j \alpha(r) \sin(\frac{r}{r_j}\psi)$$

where $r$ is the distance from the center of the jet axis. Except where the jets are launched into the domain, the boundary conditions used are extrapolation. To prevent the expansion of the jet inflow boundary with time, a ring of zero velocity that extends to $1.125 r_j$ is maintained around the jet launching region. This is done to keep the jet conditions from bleeding into the extrapolation boundary zones surrounding the jet.

Table 1: Simulation Parameters. See text for details.

| | |
|---|---|
| Jet Radius $r_j$ | 100 AU |
| Computational cells per $r_j$ | 16 |
| Jet Density $\rho_a$ | 7500 cm$^{-3}$ |
| Jet Peak Velocity $v_\circ$ | 200 km s$^{-1}$ |
| Jet Temperature | $10^4$ K |
| Ambient Density $\rho_a$ | 2500 cm$^{-3}$ |
| Ambient Temperature $T_a$ | 200 K |
| Shear parameter $s$ | 0.9 |

We have carried out two sets of simulations. Each set is defined in terms of the opening angle of the outflow, 0° and 15°. Hereafter we will use the term "jets" to refer to cases with 0° spray angle and the term "wide angle jets" (WAJ) to refer to the cases with 15° spray angle. Note that this is the half opening angle of the outflow measured from the jet axis to limit of the beam. Each simulation set has been carried out over the impact parameters $b = 0$, $b = r_j$, and with $b$ sufficiently large that the bow shocks do not intersect. We use the results of the "non-interacting" simulations as a control case to contrast with the effects of the interacting winds at smaller impact parameters. For the collimated jet non-interacting case $b = 5.33 r_j$ and the WAJ case $b = 8 r_j$.

We note that due to computational cost we were only able to follow the evolution of flows for time and length scales that are short compared to actual YSO environments. This is often the case for YSO jet simulation studies as the expectation is that scalings allow the behavior present in the simulation to characterize what occurs in YSO environments.

## 4. Results

### 4.1. Morphology

Figure 2 shows a semi-transparent volume rendering of the logarithm of gas density of the jet collision simulations for each impact parameter studied. Isosurface contours are shown at $\log\left[\rho\left(\mathrm{cm}^{-3}\right)\right] = 2.0, 3.0, 4.0,$ and 5.0. When the directly colliding jets are perfectly aligned we observe a complete redirection of the flow. The two jets merge into a single beam. The redirection occurs via the formation of oblique shocks within each beam at the point of impact. Simple momentum conservation considerations show that redirection angle, $\tan\theta = \left(\frac{\rho_2 v_2}{\rho_1 v_1}\right)$ where $\rho_1$ and $v_1$ are the density and velocity of the initial jet in the $\hat{x}$ direction and $\rho_2$ and $v_2$ are the that of the initial jet in the $\hat{y}$ direction. Because of the identical conditions in each of the orthogonal jets considered here, the resulting flow exits at an angle of $\theta = 45^o$ from either jet axis. Note that the resultant jet beam emanating from the point of impact has a small opening angle and hence its radius throughout the computational space is smaller than that of the original jets. We find that this result is strongly dependent on radiative cooling. When the cooling is turned off completely a broader redirected flow is obtained. This result is to be expected and similar behavior was obtained in the study of conical converging flows studied by Canto et al. (1988). In particular that study derived relationships between the converging conical flow of half-angle of incidence, $i$, and the half-opening angle, $\alpha$, of the resultant flow. The resultant half-opening angle, it was found, depends on the inverse compression ratio behind the conical shock, $\zeta = \rho_u/\rho_d$, where subscripts u and d refer to upstream and downstream conditions.

$$\tan\alpha = \frac{(1-\zeta) - \sqrt{(1-\zeta)^2 - 4\zeta\tan^2 i}}{2\tan i} \tag{2}$$

The equation above demonstrates that as the compression ratio increases (and $\zeta$ decreases), the opening angle of the conical axial shock will decrease. This result also applies to the opening angle in the plane of symmetry of the resultant flow emerging from the direct interaction of jet outflows. As $\alpha$ decreases, the radius of the emerging jet at any point downstream drops as well. The post-shock compression depends on the degree of radiative cooling. Thus equation 2 predicts that the secondary outflow forming from collisions of incident streams will become more narrow with more effective cooling. The shock bounded slab at the vertex of the interaction region of the simulations presented here achieves $\approx 24\times$ compression. The predicted half opening angle is then $\alpha \approx 2.6°$. The simulations (figure 4) reveal a half-opening angle $\approx 2.7°$, consistent with the analytic prediction.

While the $b = 0$ case produces strong modification of the jet flow, the grazing collision

case, $b = 2r_j$, has far less dramatic morphological consequences. Consideration of figure 2 shows that no global redirection of material occurs in the $b = 2r_j$ case and only a minor "splash" of slowly moving post-shock material is dragged away from the bow shocks surrounding the two jet beams. Comparison of the $b = 2r_j$ case with the control case shows little morphological difference. Thus, in terms of modifying the global flow for narrowly collimated jets with strong cooling, impact parameters of $b < 2r_j$ are required to significantly alter the morphology of the system.

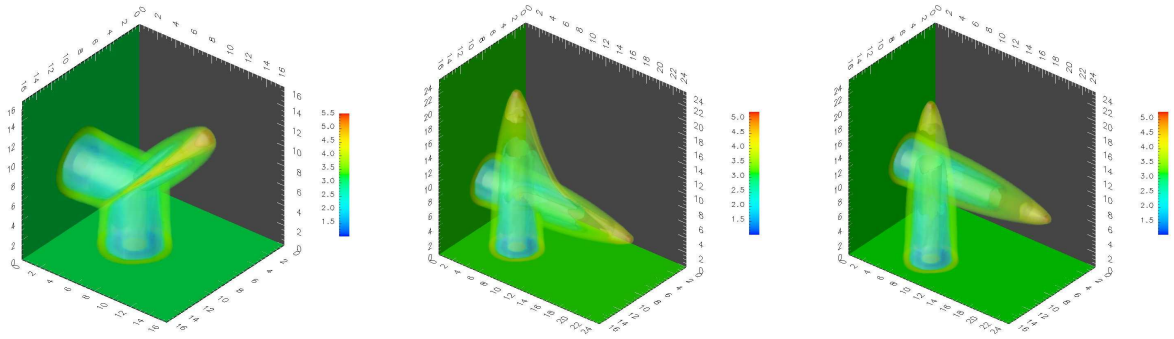

Fig. 2.— A semi-transparent volume rendering of gas density in units of $\log(\mathrm{cm}^{-1})$ at time $t = 75$ yr for the collimated jet simulations. Semi-transparent isosurfaces are plotted at $\log(\rho) = 2.0, 3.0, 4.0, 5.0$ cm$^{-1}$. The axes are labeled in units of $r_j = 100$ AU. Impact parameters of $b = 0$ (left), $b = 2r_j$ (center), and $b = 5.33r_j$ (right) are shown.

Figure 3 presents the results for the WAJ simulations for each impact parameter. Figure 3 uses the same visualization technique described for the collimated jet case. Note that the leading edge of the WAJ outflows are driven by an increasingly diluted wind as the flow evolves due to geometrical effects. As in the collimated jet case we see that a direct collision ($b = 0$) yields a compete redirection of the flow. Once again we see a new, merged flow extending from the point of impact of the two incident beams. As in the fully collimated jet collision we also see a resulting flow with a smaller radii than that for the incident beams. A significant difference exists between the collimated and WAJ case however in the nature of the internal dynamics of the collision. The collision of the two flows always creates a shock bounded sheet of gas which, because of the strong cooling, flows almost parallel to the shock tangents. In the study of colliding flows the region between the shocks is often called a cold dense layer (CDL) (Walder & Folini 2000). The WAJ collision leads to the creation of broader CDL than in the collimated jet case. This is simply due to the larger surface area associated with a conic section through the cone of a WAJ as compared with that for the cylindrical beam of the collimated jet. Cross cuts about the symmetry plane for the $b = 0$ collimated jet (figure 4) and WAJ (figure 5) cases show that the density of the redirected

flow in the CDL is greatly enhanced across the shock, as expected.

Consideration of the larger impact parameter simulation shows an additional significant difference between the collimated and WAJ simulations. The wide spray angle (15°) of the WAJ simulation results in strong interaction of the injected beams in the $b = 2r_j$ case. Figure 3 shows that material in the beam of each WAJ is caught up in the collision. A more detailed examination of the results shows that nearly half of the material injected by each WAJ participates in the interaction.

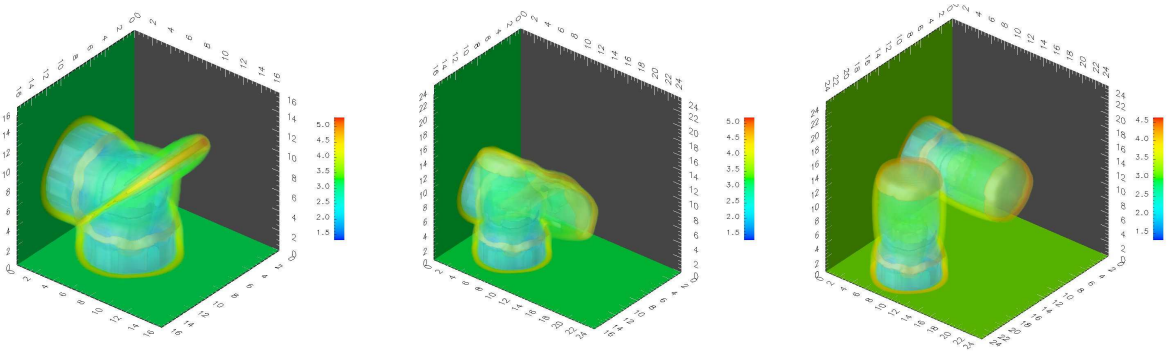

Fig. 3.— A semi-transparent volume rendering of gas density in units of $\log(\mathrm{cm}^{-1})$ at time $t = 75$ yr is shown for the WAJ simulations. Semi-transparent isosurfaces are plotted at $\log(\rho) = 2.0, 3.0, 4.0, 5.0$ cm$^{-1}$. The axes are labeled in units of $r_j = 100$ AU. Impact parameters of $b = 0$ (left), $b = 2r_j$ (center), and $b = 8r_j$ (right) are shown.

### 4.2. Entrainment of Ambient Gas and Turbulence

In this section we attempt to extract more quantitative measures of the interacting jet's ability to excite motions of ambient material. One of the most frequently used diagnostics for ambient mass entrainment are mass-velocity relations. Molecular outflows associated with YSOs often exhibit power law mass distributions as a function of velocity, $M(V) = V^{\gamma}$, at low and intermediate flow velocities. A break in the power-law is often present at the highest velocities associated with the speed of the outflow driver. As noted in the introduction it remains unclear if the driver is a protostellar jet or wide angle wind though the driver speed is usually close to the escape velocity of the protostar ($V \sim V_{esc} \sim 100$ km s$^{-1}$).

In Figure 6 we show the $M$vs. $|V|$ plots extracted from our simulations. The $M$vs. $|V|$ data is extracted from the simulations by binning the gas in the computational domain into 2 km s$^{-1}$ wide channels. The distribution of ambient mass is displayed in histogram form as a function of velocity for each impact parameter in separate plots for the collimated jet and

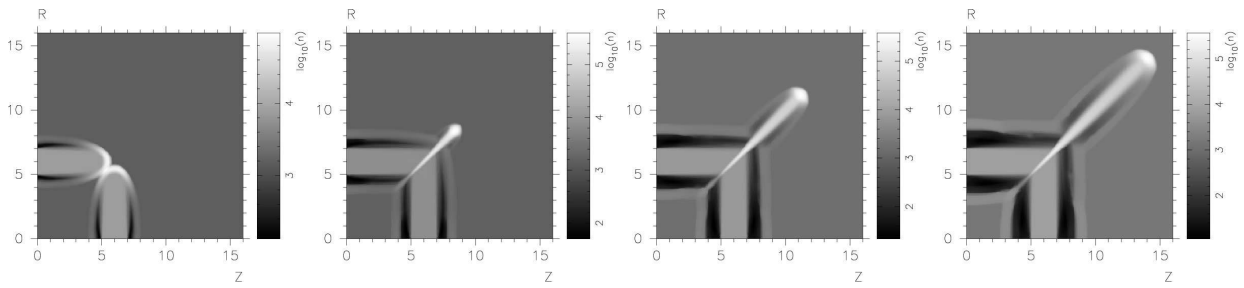


Fig. 4.— Cross sections about the plane of symmetry for the collimated jet direct collision ($b = 0$) simulation of gas density in units of $\log(\mathrm{cm}^{-1})$ are shown at time $t = 18.75, 37.5, 56.25, 75$yr from left to right. The axes are labeled in units of $r_j = 100$ AU.

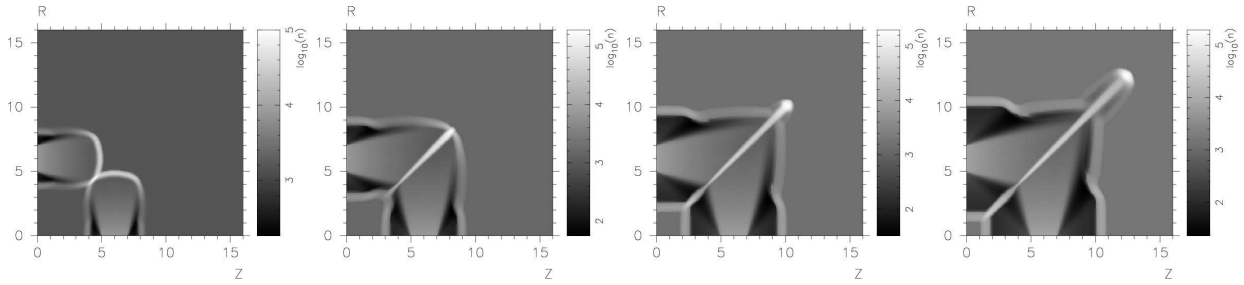


Fig. 5.— Cross sections about the plane of symmetry for the WAJ direct collision ($b = 0$) simulation of gas density in units of $\log(\mathrm{cm}^{-1})$ are shown at time $t = 18.75, 37.5, 56.25, 75$ yr from left to right. The axes are labeled in units of $r_j = 100$ AU.

WAJ cases. It is clear from the figures that in the collimated jet cases the interaction does not disrupt the power law behavior of these flows at intermediate velocities. The collimated outflow simulations produce good fits to a power law at intermediate velocities with an index of $\gamma \sim -1.7$. This is value is consistent with both observational (Lada & Fich 1996) and theoretical (Smith, Suttner, & Yorke 1997; Lee et al. 2001) studies which find a range of $\gamma \approx -1.3$ to $-2.5$ for both YSO jet flows and wide angle winds at later stages in their evolution. Note that wide angle winds can produce these power law distributions only in cases in which the ambient medium shows a strong toroidal density distribution and/or the wind shows significant asphericity in terms of its pole to equator momentum distribution Li & Shu (1996); Gardiner et al. (2003). In the WAJ case we do not see such clean power law behavior at lower velocities. We attribute this difference to the fact that we are not using a wide angle wind in the sense discussed above. The momentum distribution in the jet is not a function of polar angle and the ambient density is constant.

The most important result in the present context, however, is the fact that we see no

significant differences, in either the collimated jet or WAJ cases, between simulations with different impact parameters. The outflow collisions have not greatly enhanced the amount of ambient material entrained into the flow, nor has it accelerated a significant fraction of ambient material to high velocity. The interacting cases have accelerated only a small fraction of the outflow material to $v \sim 100$ km s$^{-1}$ when compared to the non-interacting control case. The shape of the $M(v)$ curves at velocities $v < 60$ km s$^{-1}$ in all cases are similar. Only at higher velocities do we see any difference between the various impact parameters. For the direct collision collimated jet simulation we find a local maximum in mass occurring at $V \sim$ 100 km s$^{-1}$ due to the redirected jet material. The local maximum corresponding to redirected outflow material in the WAJ $b = 0$ and $b = 2r_j$ cases occurs at $V \sim 125$ km s$^{-1}$.

The excitation of motions of a variety of scales must occur if outflows are to act as the sources of turbulent energy for the parent cloud. It might have been expected that the collision of high speed outflows would be effective at entraining more ambient material into the flow while isotropizing the momentum of the jets. This could happen if collisions increased the efficiency and rate of momentum exchange with the environment, relative to the non-interacting case, by redirecting post-collision material into a wide spray which generated motions on a variety of scales. Our simulations show no evidence that jet collisions with radiative losses create a wide spray or accelerate more material than in the non-interacting case. Excluding the local maxima noted previously, the direct collision cases have entrained less ambient material at all velocities compared to the non-interacting and weakly interacting cases (figure 6). We attribute this to the reduced bow shock surface area where ambient material is entrained into the flow. The strong cooling present behind the collision shock allows the redirected outflowing material to condense into a thin column (figure 5). The net surface area of this column is less than what is realized in the absence of the collision. The strong dissipational nature of the direct collision means that we have effectively taken two jets with the associated capacity to entrain ambient gas and turned them into a single denser, more narrow outflow.

### 4.3. Enstrophy Generation

The route to turbulence is expected to take the form of an excitation of modes on a variety of scales. In the classical theory of incompressible turbulence (Kolmogorov 1991) these modes are vortices of different eddy size. A self-similar cascade of vortical motions from the injection scale down to the dissipation scale is expected to be the final steady state of sustained turbulence. Thus we expect to see enhanced enstrophy within the computational domain as a precursor to the development of turbulence. Enstrophy will be injected into the

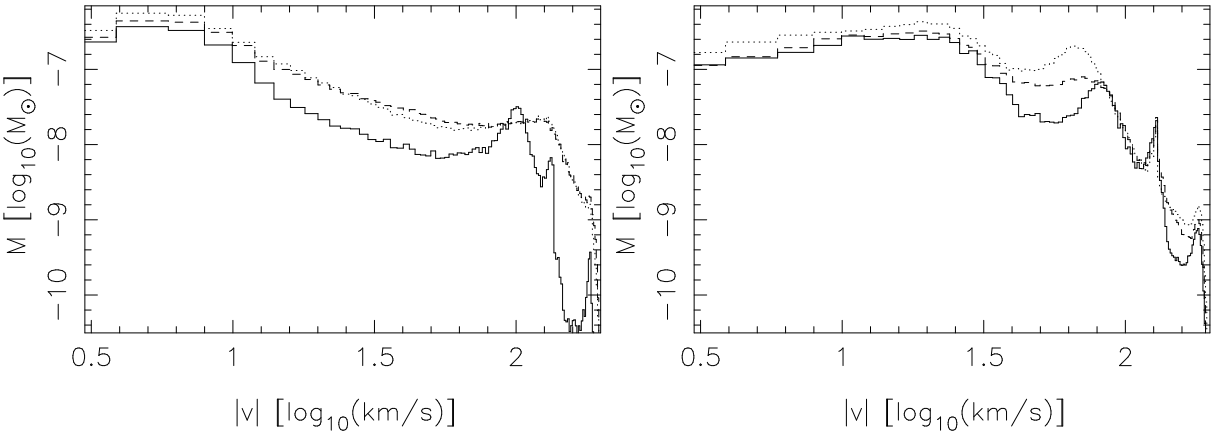


Fig. 6.— Ambient gas mass vs. velocity magnitude power law histograms at $t = 75$ yr are for the collimated jet (left) and WAJ (right) simulations. Solid lines correspond to direct collision, dashed lines correspond to impact parameter $b = 2r_j$ and dotted lines correspond to the non-interacting case.

the domain at rate proportional to the shear within the jet-bow shock complex. This can be estimated using a model for the growth of the bow shock in both the lateral and transverse dimensions. A number of authors have provided analytical models for the shape of a jet driven or clump-driven bow shock (Raga & Bohm 1985; Cabrit et al. 1997). In Ostriker et al. (2001) a thin shell model was presented. In these models the width of the bow shock, $r$, took the following asymptotic form when the height of the jet $z$ was much larger than $r_j$

$$z(r) \sim \left(\frac{r}{r_j}\right)^3 (v_s r_j)(3\beta c_s) \tag{3}$$

Where $v_s$ is the speed of the jet head, $c_s$ is the post shock sound speed and $\beta$ is a term of order unity reflecting the effect of cooling on transverse momentum exiting the jet head. Using the simple time dependence $z = v_s t$ one finds for that the maximum bow width $r_{max}$ (at the base of the flow) grows as

$$r_{max} = (3\beta c_s r_j)^{1/3} t^{1/3} \tag{4}$$

A simple estimate of the vorticity magnitude then comes from integrating the shear in the bow shock over a the bow shock shape.

$$|\omega| = \frac{\partial v_z}{\partial R} \sim \frac{v_j}{r_{max}} \tag{5}$$

The total magnitude of vorticity in the grid then becomes

$$|\Omega| = \int |\omega| \, dV = 2\pi \int_{z=0}^{v_s t} \int_{r=0}^{r_{max}} r \, |\omega| \, dr dz \tag{6}$$

which can be evaluated to

$$|\Omega(t)| = Ct^{4/3} \tag{7}$$

Thus for a single jet we expect the total average enstrophy injected into the grid to increase as a power law $t^n$ in time with $n > 1$.

Figure 7 shows the sum of the magnitude of vorticity generated in the simulation domain as a function of time. We have integrated the enstrophy over the whole domain for each case. First, for the collimated jet cases, we note that the non-interacting case exhibits a power law behavior, as derived above, with $n \approx 1.1$. Consideration of the directly interacting cases shows them to be less effective at feeding enstrophy into the grid than the non-interacting case. Thus, the bulk of the enstrophy in an unperturbed jet does arise from shear across the jet/bow cross section. Fig 7 shows that the non interacting WAJ case generates slightly more enstrophy than the collimated jets. This effect can be attributed to their larger bow shock surface area.

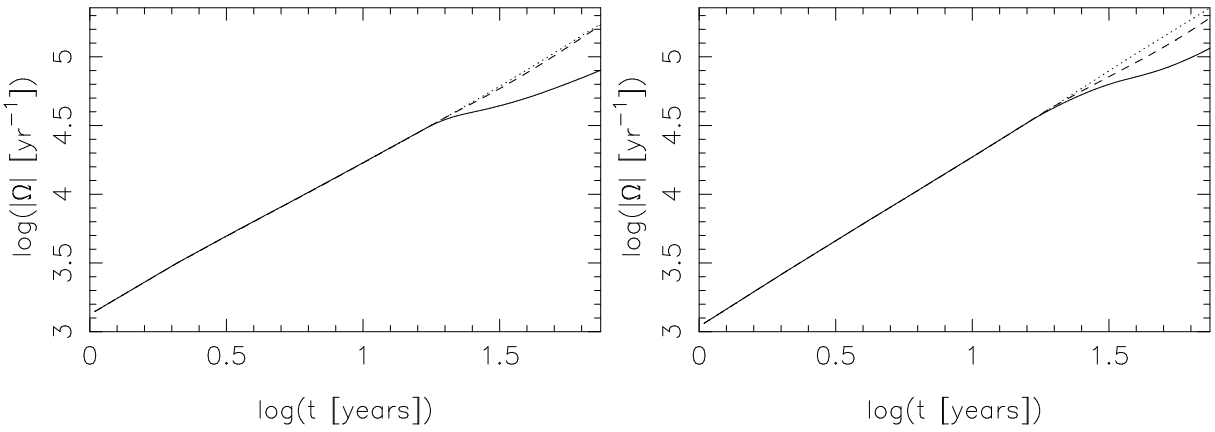


Fig. 7.— The sum of the vorticity magnitude generated in the simulation domain as a function of time for the collimated (left) and WAJ (right) simulations. Solid lines correspond to direct collision, dashed lines correspond to impact parameter $b = 2r_j$, dotted lines correspond to the non-interacting case.

### 4.4. Radiative Energy Loss

We apply the normal adiabatic shock jump conditions at the head of the bow shock to estimate the radiative energy loss achieved through the action of a single jet. The post bow shock temperature $T_{bs}$ is given in the strong shock limit by $\frac{T_{bs}}{T_{amb}} = \frac{2\gamma(\gamma-1)}{(\gamma-1)^2}\left(\frac{v_{bs}}{c_{amb}}\right)^2$ where $c_{amb} = 1.3$ km s$^{-1}$ is the ambient sound speed and $v_{bs} = \frac{v_j}{1+(\rho_j/\rho_{amb})^{-1/2}}$ is the estimate of the

bow shock propagation speed of Blondin et al. (1990). Taking the parameters for the flows presented here (table 1) we calculate $v_j = 140$ km s$^{-1}$ and $T_{bs} = 7.2\times10^5$ K. The temperature in the post shock region falls quickly behind the the bow shock to $T \sim 10^4$ K. Therefore, most of the thermal energy generated across the shock front is lost to radiation. The percentage of energy injected into the grid that is lost through shock heating and subsequent cooling within an annulus of cylindrical radius $r_j$ is given by $\frac{E_{rad}}{E_{injected}} = \frac{3\rho_{bs}RT_{bs}}{\rho_j v_j^2 + 3\rho_j RT_j}\frac{v_{bs}}{v_j} = 0.2$ where the gas density immediately behind the bow shock in the strong shock limit is $\rho_{bs} = \frac{\gamma+1}{\gamma-1}\rho_j$ and $R$ is the gas constant. We emphasize that this calculation includes only the dominant source of radiative loss at the head of the bow shock and excludes the radiative losses across the inner wind shock nor does it include radiative losses along the oblique edges of the bow shock. This result is therefore a lower-limit prediction of the radiative energy loss due to the propagation of non-interacting jets. The fractional radiative loss achieved in our simulation of non-interacting jets is $\sim 0.25$ (figure 8), in agreement with this result.

The direct collision of outflow streams results in significant additional energy lost through radiation relative to the non-interacting case. The fraction of the total energy budget invested into the domain that has been emitted as radiation as a function of time is shown in figure 8. In the collimated jet case, the direct collision of the outflow streams doubles the radiative energy loss. This accounts for more than half of the total energy imparted to the outflow. The WAJ cases produce slightly greater radiative losses than their collimated jet counterparts owing to the larger working surface at the head of the outflow. The increased radiative losses achieved through collisions reduces the energy budget available for driving turbulent motions after the driving source has expired and the flow has been subsumed into the parent cloud.

### 4.5. The Adiabatic Case

To quantify the effect of radiation on outflow collisions we have performed collimated jet collisions simulations using a polytropic equation of state for a monotonic gas with impact parameters $b = 0$ and $b = 8r_j$ (figure 9). Because the pressure behind the bow shock is not lost through radiation, the bow shocks are wider than in the radiative cases. Note that the flows in the $b = 8r_j$ case do interact slightly. Approximately 30% of the injected flows' cross sectional area overlap at the widest point of the bow shock. As we have noted earlier, such grazing collisions have little measurable effect on the global flow. The morphology of the resultant flow in the direct collision case is markedly different from the radiative cases. The thermal energy deposited into the flow at the collision shock is retained and the thermal pressure in this region is dynamically significant. Because the thermal pressure drives the

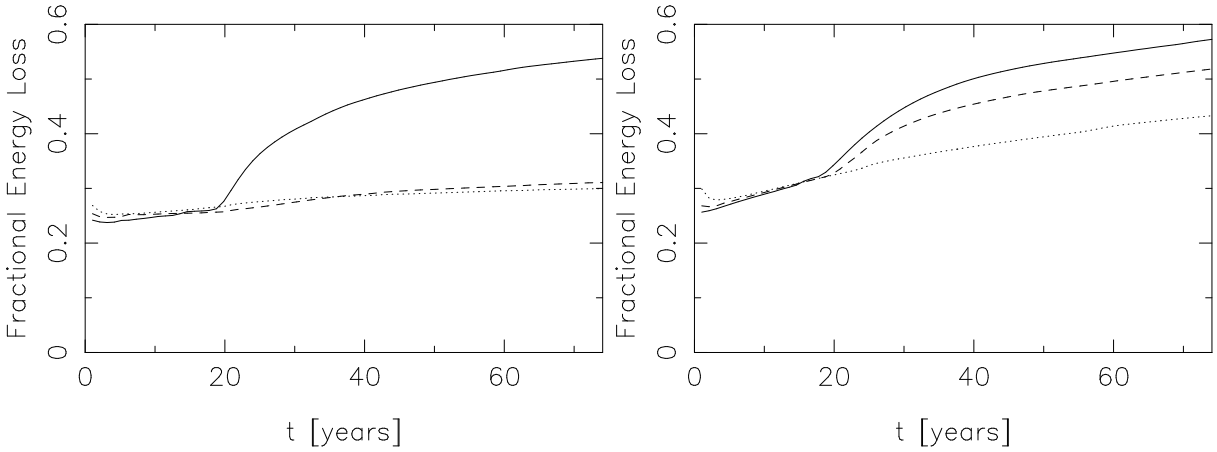


Fig. 8.— Fraction of total energy loss through radiation for the collimated (left) and WAJ (right) simulations. Solid lines correspond to direct collision, dashed lines correspond to impact parameter $b = 2r_j$, dotted lines correspond to the non-interacting case.

flow isotropically, the resultant flow has a comparable spatial extent in all three dimensions and is driven over a considerably larger volume than in the radiative case.

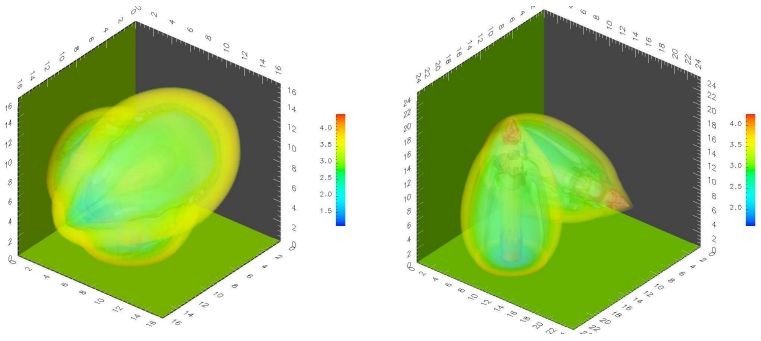

Fig. 9.— A semi-transparent volume rendering of gas density in units of $\log(\mathrm{cm}^{-1})$ at time $t = 60$ yr for the adiabatic collimated jet simulations. Semi-transparent isosurfaces are plotted at $\log(\rho) = 2.0, 3.0, 4.0$ cm$^{-1}$. The axes are labeled in units of $r_j = 100$ AU. Impact parameters of $b = 0$ (left), and $b = 5.33r_j$ (right) are shown.

In figure 10 we show the ambient mass distribution as a function of the magnitude of the flow velocity at the end of the adiabatic simulations. The adiabatic flows reveal a much steeper power law dependence over a narrower range of velocity ($|v| \sim 50 - 100$km s$^{-1}$) than the radiative case. Comparing the radiative mass distribution (figure 6) to the adiabatic, we note that the adiabatic collision has resulted in considerably more ambient material entrained into the flow at lower velocity. Because the resultant flow consumes a larger volume, considerably more material can be entrained into the flow if radiative losses are

suppressed.

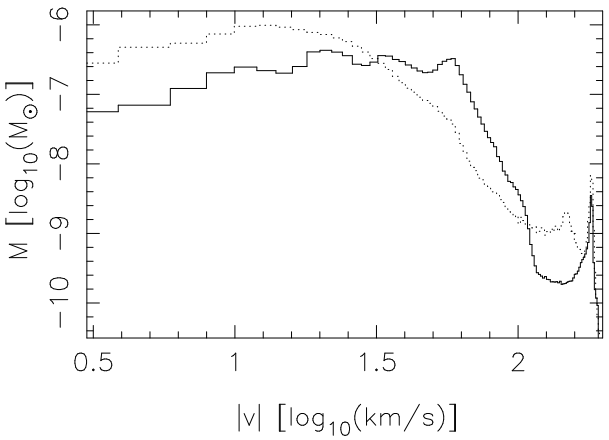


Fig. 10.— Ambient gas mass vs. velocity magnitude histograms at $t = 60$ yr are shown for the adiabatic collimated jet simulations. Solid lines correspond to direct collision and dotted lines correspond to the non-interacting case.

## 5. Discussion

### 5.1. Result Summary

The direct collisions have the least potential to drive turbulence in their environment. The two injected streams merge into a single redirected flow across a "collision shock" at the vertex of the interaction region. The redirected outflow is condensed into a narrow, high density flow owing to strong radiative cooling. The gas compression achieved by the action of the radiative collision shock allows the redirected flow to remain within a more spatially confined region than if the flows did not collide. The surface area of the bow shock driven by the advance of the redirected flow is less than what is realized in the absence of collision. The reduction of the net surface area of the advancing bow shock is responsible for the reduced rate of entrainment of ambient material into the flow. A significant fraction of the energy of the outflow streams is radiated away in the post-collision shock region. The resultant outflow has reduced energy budget to contribute to the turbulent energy of the region.

The indirect, $b = 2r_j$, collisions have little effect on the outflows' potential to drive turbulence. While the driving winds in the WAJ $b = 2r_j$ case interact, only the fraction of material in the intersecting outflow limbs pass through a collision shock and the driving winds do not merge into a completely redirected flow. Grazing collimated jets interact through the lateral edges of the bow shock. In this case, the injected gas streams are not redirected.

Only the cocoon of shocked material between the jet and bow shocks is disrupted by the collision. The lateral edges of the bow shock that participate in the collision contain only a small fraction of the momentum of the overall outflow which is not sufficient to produce any significant effect on the entrainment or deposition of momentum into ambient material. The vorticity produced within the shear layer around the working surface at the head of the outflow is spatially redistributed but not significantly enhanced through the interaction.

### 5.2. Statistics of Global Cloud Support

In §1, we estimated the stellar density necessary to achieve an appreciable number of protostellar outflow collisions. However, the results of this work have shown that only low impact parameter collisions where the high speed, preshock outflow gas streams collide directly are able to disrupt the global characteristics of the flow. To estimate the stellar density required to achieve a significant number of direct collisions, we repeat the calculation setting $R = 200$ AU, characteristic of the radial extent of the preshock outflow streams. This yields a critical density for direct collisions of $N_{critical}^{direct} = 5 \times 10^6$ pc$^{-3}$. Such a stellar density is three orders of magnitude higher than the most dense star forming regions. Thus the direct collision of preshock outflow material is unlikely. While protostellar outflow collisions are likely common, the direct collision of the driving winds is not. Outflow collisions therefore do not influence the turbulent energy budget of the parent cloud on a global scale.

## 6. Conclusions

The radiative energy losses when unshocked protostellar outflow streams directly collide reduces the kinetic energy available to deposit into the molecular cloud as turbulent energy. The high degree of compression of outflow gas induced by cooling from such a collision prevents the redirected outflow from spraying over a large spatial region. Furthermore, the collision reduces the redirected outflow's ability to entrain and impart momentum into the ambient cloud. The cooling of the interaction region produces a reduced bow shock surface area over which outflow momentum can be exchanged with ambient gas. "Grazing" collisions, where only the cocoon of shock-decelerated gas or a small fraction of the high speed outflow gas collide, however, have little effect on radiative energy loss or the rate of entrainment of ambient material into the flow. Because the direct collision of protostellar outflows is rare, we conclude that such collisions have little effect on the turbulent energy budget of molecular clouds.

Based on the results of this study we conclude that if turbulence is energized by outflows it does not occur through collisions of active outflows. Instead the mechanical energy of an outflow is most likely supplied to the turbulent motions of the cloud through the action of *fossil* cavities that remain after the driving source of the outflow has expired. The role of individual or possibly overlapping fossil outflows was explored before (Quillen et al. 2005). This study focused on NGC 1333 and explored the interaction of the cloud with slowly moving shells which remain after the outflow source has either shut down or become signifigantly weakened by the decrease in $\dot{M}_j$. The fossil cavities were shown to carry significant momentum and can provide the coupling mechanism between outflow and turbulent motions in the cloud. Using the bow shock radius and outflow length in §2, without accounting for collisons, the volume fill ratio of outflow cavities exceeds unity at stellar density $> 32$ pc$^{-3}$. We speculate that as the density of protostars approaches this value, the parent cloud will become subsumed in motion driven by randomly oriented fossil cavities. Future work should focus on the interaction of fossil outflows that were launched at different times within a turbulent cloud and their overlap to unravel the exact mechanisms by which this provides a route to sustained turbulence.

This paper benefited from discussions with Alice Quillen, John Bally, Alyssa Goodman, Hector Arce and Mordecai-Mark Mac Low. We acknowledge support from the Jet Propulsion Laboratory Spizter Space Telescope theory grant 051080-001, HST theory grant 050292-001, NSF grants 0507519, AST-0406799, AST 00-98442, AST-0406823, DOE grant DE-F03-02NA00057, NASA grant ATP04-0000-0016, the Laboratory for Laser Energetics, and the Center for Computational Research at the University of Buffalo.

## REFERENCES

Arce, H. G. 2003, RevMexAA, 15, 123

Arce, H. G. & Goodman, A. A. 2001, ApJ, 554, 132

Blondin, J. M., Fryxell, B. A., & Konigl, A. 1990, ApJ, 360, 370

Bally, J., Devine, D., & Alten, V. 1996, ApJ, 473, 921

Bally, J, & Reipurth, B. 2001, ARAA, 39, 403

Cabrit, S., Raga, A., & Gueth, F. 1997, IAU Symp. 182: Herbig-Haro Flows and the Birth of Stars, 182, 163

Canto, J., & Raga, A. C. 1991, ApJ, 372, 646

Canto, J., Tenorio-Tagle, G., & Rozyczka, M. 1988, A&A, 192, 287

Chernin, L., Masson, C., Gouveia dal Pino, E. M., & Benz, W. 1994, ApJ, 426, 204

Cunningham, A., Frank, A., & Hartmann, L. 2005, ApJ, 631, 1010

Dalgarno, A., & McCray,R. 1972, ARA&A, 10, 375

Gardiner, T. A., Frank, A., & Hartmann, L. 2003, ApJ, 582, 269

Kolmogorov, A. N. 1991, Royal Society of London Proceedings Series A, 434, 9

Knee, L. B. G., & Sandell, G. 2000, A&A, 361, 671

Lada, C. J. & Fich, M. 1996, ApJ, 459, 638

Lebedev, S. V., et al. 2004, ApJ, 616, 988

Lee, C., Stone, J. M., Ostriker, E. C., & Mundy, L. G. 2001, ApJ, 557, 429

Lepp, S. & Shull, J. M. 1983, ApJ, 270, 578

Li, Z.-Y., & Shu, F. H. 1996, ApJ, 472, 211

Mac Low, M.-M., Klessen, R. S., Burkert, A., & Smith, M. D. 1998, Physical Review Letters, 80, 2754

Matzner, C. D. 2002, ApJ, 566, 302

Norman, C., & Silk, J. 1980, ApJ, 238, 158

Ostriker, E. C., Lee, C.-F., Stone, J. M., & Mundy, L. G. 2001, ApJ, 557, 443

Palla, F., & Galli, D. 1997, ApJ, 476, L35

Poludnenko, A., Varniere, P., Frank, A., & Mitran S, 2005, Springer's Lecture Notes in Computational Science and Engineering, Vol. 41

Quillen, A., Thorndike, S., Cunningham, A., Frank, A., Gutermuth, R., Blackman, E., Pipher, J., Ridge, N. ApJin press, astro-ph/0503167

Raga, A. C., & Bohm, K.-H. 1985, ApJS, 58, 201

Raga, A. C., & Canto, J. 1995, Revista Mexicana de Astronomia y Astrofisica, 31, 51

Shepherd, D. 2003, Astronomical Society of the Pacific Conference Series, 287, 333

Shu, C.W . & Osher, S. 1988, J. Comput. Phys., 77, 439

Smith, M. D., Suttner, G., & Yorke, H. W. 1997, A&A, 323, 223

Stone, J. M., Ostriker, E. C., & Gammie, C. F. 1998, ApJ, 508, L99

Sutherland, R. S., Bisset, D. K., & Bicknell, G. V. 2003, ApJS, 147, 187

Testi, L., Palla, F., & Natta, A. 1999, A&A, 342, 515

Varniere, P., Poludnenko, A., Cunningham, A., Frank, A., & Mitran S, 2005, Springer's Lecture Notes in Computational Science and Engineering, Vol. 41

Vazquez-Semadeni, E., Ostriker, E. C., Passot, T., Gammie, C. F., & Stone, J. M. 2000, Protostars and Planets IV, 3

Walder, R., & Folini, D. 2000, Ap&SS, 274, 343

Warin, S., Castets, A., Langer, W. D., Wilson, R. W., & Pagani, L. 1996, A&A, 306, 935

Williams, J. P. & McKee, C. F. 1997, ApJ, 476, 166